PROCEEDINGS OF THE ROYAL SOCIETY A MATHEMATICAL, PHYSICAL & ENGINEERING SCIENCES

Experimental investigation of the bond-coat rumpling instability under isothermal and cyclic thermal histories in thermal barrier systems

Rahul Panat and K. Jimmy Hsia

Proc. R. Soc. Lond. A 2004 **460**, doi: 10.1098/rspa.2003.1262, published 8 July 2004

10.1098/rspa.2003.1262

THE ROYAL SOCIETY

Experimental investigation of the bond-coat rumpling instability under isothermal and cyclic thermal histories in thermal barrier systems

By Rahul Panat and K. Jimmy Hsia

Department of Theoretical and Applied Mechanics and Frederick Seitz Materials Research Laboratory, University of Illinois at Urbana-Champaign, Urbana, IL 61801, USA (kjhsia@uiuc.edu)

Received 25 April 2003; revised 20 August 2003; accepted 30 September 2003; published online 20 April 2004

Reliable life-prediction models for the durability of thermal barrier coatings require the identification of the relative importance of various mechanisms responsible for the failure of the coatings at high temperatures. Studies of these mechanisms in subsystems of thermal barrier coatings can provide valuable information. In the present work, we undertake an experimental study of 'rumpling', or progressive roughening of the bond-coat (BC) surface in the bond coat–superalloy systems upon high-temperature exposure. Thermal cycling and isothermal experiments are carried out on a platinum aluminide BC, a nickel aluminide BC, and an NiCoCrAlY BC deposited on an Ni-based superalloy in air and in vacuum. Cyclic experiments are conducted in air for different levels of initial roughness of the BC surface. Upon thermal cycling in air, the BC surfaces with a wide range of initial roughness rumple to comparable characteristic wavelengths and amplitudes, indicating the insensitivity of the rumpling phenomenon to the initial surface fluctuations. Observations of the rumpled BC surfaces show that the stresses in the BC provide driving force for the rumpling process. On comparing the experimental observations with existing rumpling models in the literature, it is concluded that the thermally grown aluminium oxide and the microstructural changes in the BC have a limited role in inducing rumpling. Plausibility of several possible deformation mechanisms is discussed. It is shown that several of the rumpling observations in the current work can be explained by a BC stress-driven surface-diffusion model from the literature.

Keywords: thermal barrier coatings; surface rumpling; surface diffusion

1. Introduction

Increasing demand for higher operating efficiencies of jet engines and gas turbines has led to the development of thermal barrier coating (TBC) technology over the last two decades (Goward 1998; Meier & Gupta 1994; Miller 1987; Padture *et al.* 2002; Schulz *et al.* 2003; Sheffler & Gupta 1988; Stiger *et al.* 1999; Strangman 1985). The TBCs are multi-layered metal–ceramic coatings used to reduce the surface temperature of superalloy components in the hot sections of jet engines, gas turbines and diesel engines (Levy & MacAdam 1988; Padture *et al.* 2002; Rejda *et al.* 1999).

The higher operating temperatures made possible by TBCs result in higher engine efficiencies. For a fixed operating temperature, this translates into an improved oxidation resistance and prolonged creep life of the engine components. The anatomy of a typical TBC system consists of a ceramic topcoat, a thermally grown aluminium oxide (TGO), an intermediate (metallic) bond coat (BC) and a substrate superalloy. The BC is deposited on the superalloy, while the ceramic is deposited over the BC at high temperatures. The TGO is a reaction product that grows over the BC at high temperatures and occupies the BC–ceramic interface. The BC is typically platinum aluminide or NiCoCrAlY alloy.

In spite of the excellent advantages offered by TBCs, their long-term durability is limited, primarily due to the problems associated with ceramic topcoat spallation. Since the local temperature in the hot section of a gas turbine can exceed the melting temperature of the superalloy, this spallation can be quite dangerous. Several laboratory and field experiments have been carried out in the past subjecting different types of TBC systems to failure under isothermal, thermomechanical or cyclic thermal histories (Ambrico *et al.* 2001; Bouhanek *et al.* 2000; Ibegazene-Ouali *et al.* 2000; Mumm *et al.* 2001; Ruud *et al.* 2001; Schulz *et al.* 2001; Sohn *et al.* 2001; Tolpygo & Clarke 2001; Tolpygo *et al.* 2001; Vaidyanathan *et al.* 2000; Wright 1998; Wu *et al.* 1989). Although the TBC failure under thermal loading is seen to vary from system to system (e.g. Bouhanek *et al.* 2000; Ruud *et al.* 2001; Schulz *et al.* 2001; Tolpygo & Clarke 2001; Tolpygo *et al.* 2001), some general trends can be established.

Typically, the failure process is associated with morphological instabilities, or 'rumpling', occurring at the BC–ceramic interface, with the TGO inbetween (Evans *et al.* 2001; Wright & Evans 1999). Aspects of the rumpling phenomenon have previously been explored through experimental studies on TBC subsystems consisting of the substrate coated with BC only (Deb *et al.* 1987; Holmes & McClintock 1990; Pennefather & Boone 1995; Tolpygo & Clarke 2000; Zhang *et al.* 1999). Platinum aluminide, nickel aluminide and NiCoCrAlY BCs deposited on superalloy substrates rumple to wavelengths ranging from *ca.* 40 μm (Tolpygo & Clarke 2000) to *ca.* 300 μm (Pennefather & Boone 1995) upon thermal cycling to temperatures up to 1200 °C. The amplitude of the rumpled surfaces in these experiments was up to 15 μm. Under isothermal experiments at 1100 °C (Deb *et al.* 1987) and at 1150 °C (Tolpygo & Clarke 2000), no rumpling was observed. Under fast heating and cooling rates (a temperature change from 1050 to 300 °C in about a minute) along with mechanical loading of the superalloy substrate, the BCs were seen to rumple (see Holmes & McClintock 1990; Zhang *et al.* 1999) with additional thermal shock effects such as 'scalloping' (Holmes & McClintock 1990), or large-scale spallation of the TGO.

The critical questions to understanding the instability-related failure process in TBCs are as follows.

(i) What are the deformation mechanisms responsible for such rumpling of the BC–ceramic interface?

(ii) What is the driving force for such deformation mechanisms?

Models for rumpling instabilities have been developed for generic metal-oxide systems (He *et al.* 2000; Karlsson & Evans 2001; Suo 1995), for specific BC–superalloy systems (Tolpygo & Clarke 2000), and for metallic coating–substrate systems (Panat *et al.* 2003), in which different mechanisms have been proposed to explain the experimental observations.

Some of these models emphasized the role played by the TGO. He *et al.* (2000) proposed that plastic ratcheting of the BC due to the mismatch stresses in the developing TGO during thermal cycling is responsible for the rumpling. Such a mechanism requires that the initial amplitude of surface fluctuation be larger than a critical value. Moreover, to generate plastic ratcheting, cyclic thermal history is a necessary condition for rumpling to occur. Further numerical studies by Karlsson & Evans (2001) and numerical and analytical studies on an idealized rumple geometry by Karlsson *et al.* (2002) elucidated the role of BC reverse yielding and TGO yield in inducing the TGO stress-driven rumpling (He *et al.* 2000). Suo (1995), on the other hand, suggested that the highly compressive stresses in the TGO (of the order of GPa) would provide the driving force necessary for the metal atoms to diffuse along the TGO–metal interface, leading to a wavy metal surface. Suo (1995) estimates that this mechanism would result in a rumpling characteristic wavelength of a few times the thickness of the TGO, roughly an order of magnitude smaller than that observed in experiments by Tolpygo & Grabke (1994). It is noted that the mechanisms proposed by He *et al.* (2000) and by Suo (1995) are generic for all metal-oxide systems, regardless of whether there exists an intermediate BC layer. Other models concern the microstructural changes in the BC during high-temperature testing. Based on their experimental observations, Tolpygo & Clarke (2000) suggested that the rumpling in BC–superalloy systems occurs as a result of differential diffusion of various constituents, like Ni and Al, perpendicular to the BC surface. In order to verify this mechanism, however, one needs to quantitatively demonstrate the correlation between microstructural features, such as composition variations, and surface rumpling features. Recently, Panat *et al.* (2003) developed a model based on the assumption that the stress in BCs is the driving force for the BC surface atoms to diffuse, and will give rise to rumpling with characteristic wavelengths decided by the energetics of the process, i.e. a balance between strain energy and surface energy of the BC. Among all the mechanisms proposed by the above models, it is unclear, from the experimental data available to date, which mechanism is (or which mechanisms are) dominant during the rumpling process.

Present work is inspired by the experimental observations of BC surface rumpling (Deb *et al.* 1987; Holmes & McClintock 1990; Pennefather & Boone 1995; Tolpygo & Clarke 2000; Zhang *et al.* 1999) and theoretical predictions by various models (He *et al.* 2000; Panat *et al.* 2003; Suo 1995; Tolpygo & Clarke 2000), and tries to shed light on the issue. A detailed experimental study of the rumpling of BC–superalloy systems subjected to isothermal and cyclic thermal heat treatments in air is performed. Both platinum aluminide and NiCoCrAlY bond-coated superalloy are considered. The results demonstrated that rumpling of comparable patterns occurs under a wide range of conditions, such as isothermal and thermal cycling with drastically different initial surface fluctuations. An experiment with a nickel aluminide BC subjected to an isothermal condition in vacuum is also presented. This result shows that the rumpling can occur in the absence of significant TGO. Microstructural examinations reveal poor correlation between microstructural changes and rumpling peak/valley locations. Several of the current experimental results can be explained by assuming the mechanism proposed by Panat *et al.* (2003), i.e. rumpling due to BC surface diffusion driven by BC mismatch stress. Findings in the current work point to the need for 'mechanism maps' showing the dominant mechanisms active in different thermal barrier systems under different temperature histories.

2. Experimental procedure

The substrate material used in the BC–superalloy systems in the current study was René N5, an Ni-based superalloy provided by General Electric Aircraft Engines (Cincinnati, OH). The superalloy samples were 5 mm × 5 mm × 22 mm in dimension. One of the surfaces of these samples was polished successively down to 1 μm diamond paste to remove initial surface roughness prior to BC deposition. Two types of BC materials, NiCoCrAlY and platinum aluminide, were deposited on the superalloy by the Chromalloy Gas Turbine Corporation (Orangeburg, NY). The platinum aluminide BC was deposited by electroplating a Pt layer followed by a vacuum heat treatment and a vapour-phase aluminization. The NiCoCrAlY BC was deposited by the electron beam–physical vapour deposition (EB–PVD) method. Each of the BC–superalloy samples were cut further using a wafering blade (Buehler, Lake Bluff, IL) into cubes of *ca.* 5 mm × 5 mm × 5 mm. During the cutting process, each sample was protected by embedding it in an acrylic mount. The mount was then removed using acetone.

To observe the effect of surface texture on rumpling, three types of surface morphologies were induced on each type of BC surface. In the first type, the BC surface was polished successively down to 1 μm diamond paste to produce a highly smooth surface. The second and the third types of BC surface were polished by 60 grit and 600 grit SiC papers (Buehler, Lake Bluff, IL). In the case of the platinum aluminide BC, an as-deposited surface was also used for comparison. The specimens were subjected to thermal cycling or isothermal heat in air. The thermal cycles, 25 in number, consisted of heating the specimens to 1200 °C in 55 min, a hold time of *ca.* 50 min at 1200 °C, followed by air cooling to 200 °C in 25 min. Isothermal experiments were carried out on platinum aluminide BC at 960, 1100 and 1175 °C with a hold time of 100 h and also at 1200 °C with a hold time of 25 h. The hold time at 1200 °C was chosen so as to be approximately equal to the total time at high temperature for the cyclic experiments. The choice of the other temperatures and hold times for isothermal experiments is explained in § 4. For uniformity, the surfaces of all the BC samples used in isothermal experiments in air were polished successively down to 1 μm diamond paste. A specimen with nickel aluminide BC was also subjected to isothermal exposure at 1200 °C for 25 h in vacuum (10^{-6}–10^{-8} Torr) environment.

A box furnace (Vulcan 3-400HTA, NEYTECH, Bloomfield, CT) was used to carry out all the experiments in air. A tube furnace (HTF55322A, Lindberg/Blue M, Asheville, NC) along with a quartz tube was used to carry out the experiment in vacuum environment. The quartz tube that carried the specimens ran through the tube furnace. The tube was connected to a roughing pump/diffusion pump assembly to produce a vacuum of 10^{-6}–10^{-8} Torr at 1200 °C. The temperature during the experiments was measured using a K-type thermocouple (Omega, Stamford, CT) calibrated using an optical pyrometer (The Pyrometer Instrument Company Inc., Northvale, NJ). The estimated error in the temperature measurement was *ca.* ±0.75% when measured in °C. Some of the samples were cut and their cross-section polished successively down to 1 μm diamond paste to observe the microstructural changes. The samples were examined using scanning electron microscopy (SEM), the semi-quantitative elemental analysis tool of energy-dispersive X-ray spectroscopy (EDX), and profilometry.

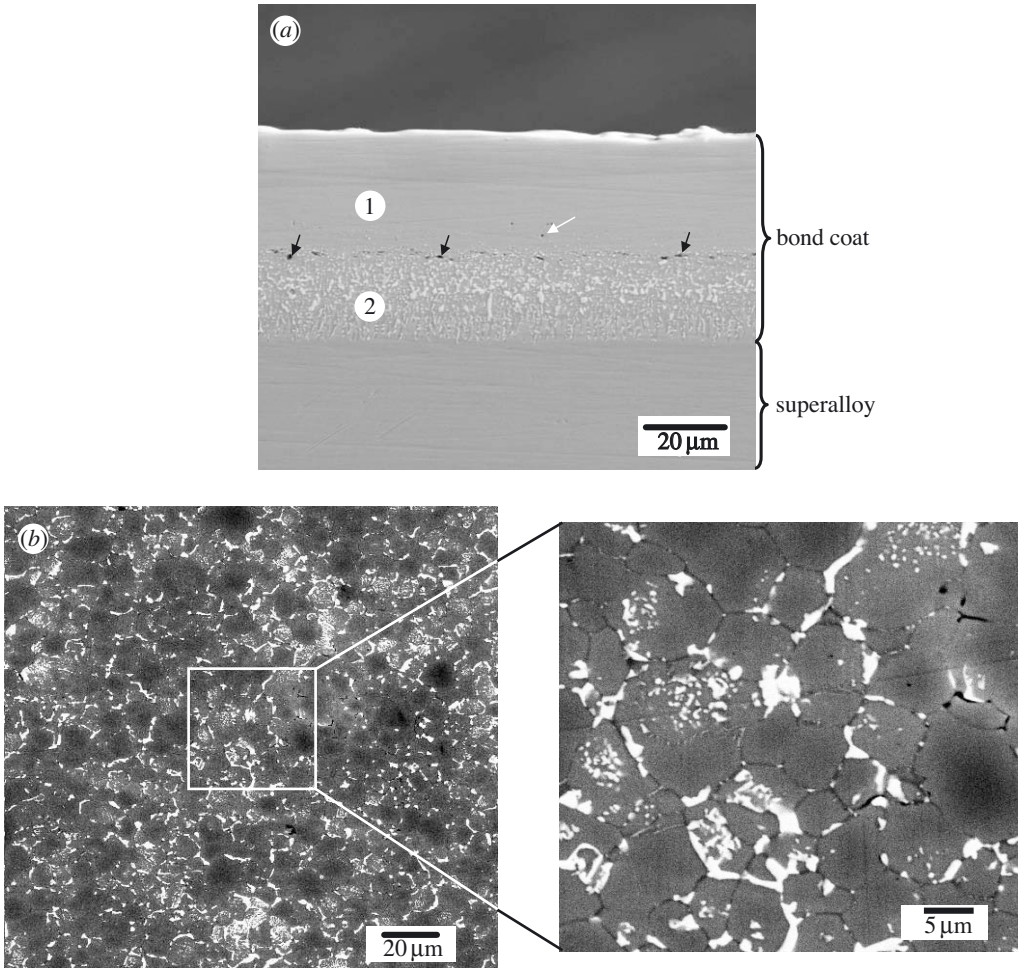

Figure 1. Microstructure of platinum aluminide BC prior to thermal cycling. (*a*) Cross-sectional SEM micrograph showing outer zone (labelled '1') and interdiffusion zone (labelled '2'). Black arrows show alumina inclusions irregularly placed between the two regions, while the white arrow shows a pore seen intermittently in the outer region. (*b*) SEM micrograph (with backscatter electrons) of the top surface polished to 1 µm diamond paste.

3. Experimental results

(*a*) *Initial microstructure and composition*

Representative SEM images of the platinum aluminide BC are shown in figure 1. Figure 1*a* shows the cross-section of the platinum aluminide BC having an outer zone (region 1) and an interdiffusion zone (IDZ) (region 2). The nominal composition of the BC is (wt%) 17Al–3.4Cr–5.9Co–34Pt–balance Ni, as determined by EDX analysis. The BC is β-Ni(Pt)Al with the IDZ containing precipitates (bright regions in figure 1*a*) rich in refractory elements (W, Mo and Ta). Alumina inclusions, shown by black arrows in figure 1*a*, were irregularly placed at the border between region 1 and region 2. Occasionally, pores were observed in region 1, as indicated by the

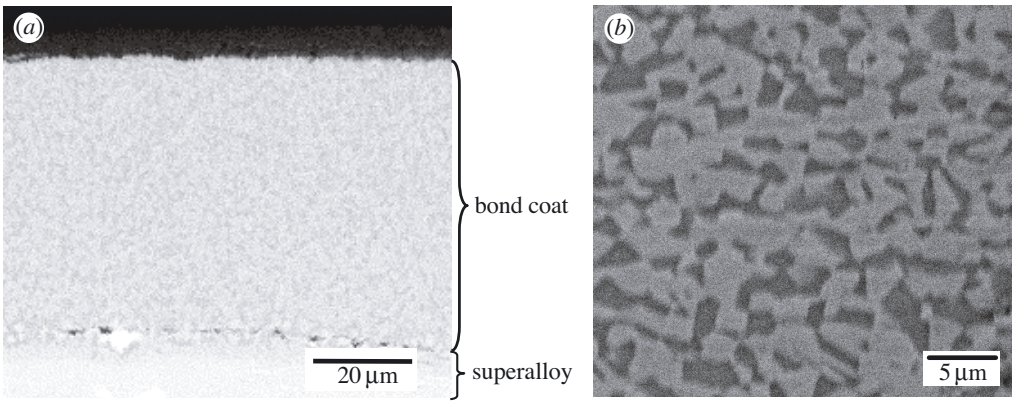

Figure 2. Cross-sectional SEM micrographs of NiCoCrAlY BC at different magnifications (*a*), (*b*) prior to thermal cycling. The randomly distributed dark and bright regions in (*b*) represent regions with an Al content of *ca.* 4 and 15 wt%, respectively.

white arrow in figure 1*a*. This structure is typical of the platinum aluminide coatings reported in the literature (Deb *et al.* 1987; Mumm *et al.* 2001; Tolpygo & Clarke 2000). The BC composition in the outer zone varied slightly in the direction perpendicular to the BC surface. Towards the top, the Al content increases (*ca.* 22 wt%), while towards the IDZ, the Al content decreases (*ca.* 15 wt%) with a concomitant increase in Co and Cr content. The nominal thickness of the IDZ was *ca.* 22 ± 2 µm, while the thickness of the outer zone varied from *ca.* 24 to 30 µm depending upon the polishing treatment of the surface. A possible effect of this variation on the rumpling behaviour is discussed in § 4. Figure 1*b* shows an SEM micrograph (with backscatter electrons) of the top surface of the platinum aluminide BC polished successively down to 1 µm diamond paste. At high magnification, BC grains of variable sizes (5–10 µm) are seen with occasional occurrences of large-sized (15–20 µm) grains. Bright regions representing secondary $PtAl_2$ can also be seen, mainly concentrated at the BC grain boundaries. These regions were present near the surface, reducing successively for thinner outer zones. Figure 2*a*, *b* shows cross-section images of an NiCoCrAlY BC at different magnifications. The randomly distributed dark and bright regions in figure 2*b* represent regions with an Al content of *ca.* 10 and 2 wt%, respectively. The composition of the René N5 superalloy (from Walston *et al.* 1996) is (wt%) 7.5Co–7Cr–1.5Mo–6.5Ta–5W–3Re–6.2Al–0.15Hf–0.05C–0.004B–0.01Y–balance Ni.

(*b*) *Rumpling observations*

(i) *Thermal cycling experiments*

Representative SEM micrographs of initial and rumpled surfaces of platinum aluminide BC under 25 thermal cycles from 200 to 1200 °C, along with the profilometer scans are shown in parts (*a*)–(*d*) of figure 3. Note that the figure designations beginning with a given letter (say '*a*') refer to the same sample. The profilometer scans in parts (*a*)(ii), (*a*)(iv), (*b*)(ii), (*b*)(iv), (*c*)(ii), (*c*)(iv), (*d*)(ii) and (*d*)(iv) correspond to the BC surfaces shown in parts (*a*)(i), (*a*)(iii), (*b*)(i), (*b*)(iii), (*c*)(i), (*c*)(iii), (*d*)(i) and (*d*)(iii), respectively. All scans have the same scale along the vertical axis for

comparison. Further, the scan lengths have been chosen to be identical to the actual width of the SEM pictures. Figure 3*a*(i) shows a BC surface polished successively down to 1 μm diamond paste, while parts (*b*)(i), (*c*)(i) and (*d*)(i) show BC surfaces polished with 600 grit SiC paper, with 60 grit SiC paper and in an as-deposited condition, respectively. The corresponding line scans in parts (*a*)(ii), (*b*)(ii), (*c*)(ii), (*d*)(ii) show surface fluctuations with a peak-to-valley distance of *ca.* 0.02 (not seen at the scale shown), 0.25, 3 and 2.5 μm, respectively. On subjecting these samples to 25 thermal cycles, the BC surfaces develop waviness, as seen in parts (*a*)(iii), (*b*)(iii), (*c*)(iii) and (*d*)(iii) with peak-to-valley distances of *ca.* 4–5, 10, 6 and 8 μm, respectively. Note that the scans for the BC surfaces polished with SiC grit (parts (*b*)(i), (*c*)(i)) are perpendicular to the polishing direction. The characteristic wavelengths of the rumples for all the samples can be seen to be *ca.* 60–100 μm. It is interesting to see that the amplitudes of the initial waviness of the BC samples varied over two orders of magnitude, while those after thermal cycling were of the same order of magnitude. Parts (*a*)(i)–(iv) indicate that significant initial defects on the BC surface were not needed for rumpling to occur. Further, the rumpling pattern seen in parts (*b*)(iii) and (*c*)(iii) does not appear to be influenced by the initial scratching directionality of the corresponding BC surfaces (parts (*b*)(i) and (*c*)(i)). The rumples on the BC surface are randomly oriented, but have some local directionality.

Cross-sectional examination of the rumpled BC revealed additional important features of the rumpling phenomenon. Figure 4 is a cross-sectional SEM image of the rumpled surface in figure 3*a*(iii). The higher-magnification image in figure 4 reveals a 1–2 μm thick TGO layer formed over the BC. The TGO is non-uniform in thickness due to a wavy BC–TGO interface. The wavelength of this interfacial waviness is *ca.* 3–5 μm, while its amplitude is slightly less than 1 μm. Thus, the BC top surface has a smaller waviness with a characteristic wavelength a few times the TGO thickness.

The platinum aluminide BC also experienced several changes in the initial microstructure upon thermal cycling as seen from the SEM image (with backscatter electrons) in figure 5, although the presence of two distinct regions in the cross-section was similar to that before cycling, as seen in figure 1*a*. Most significantly, the upper region showed intermittent zones of Al depletion, seen as lighter regions in figure 5*b*. The Al content in these zones was *ca.* 8.5 wt% as compared with *ca.* 15 wt% in the surrounding regions. Such Al-depleted zones have been identified as γ' regions in the literature (Mumm *et al.* 2001; Tolpygo & Clarke 2000). The Al depleted from these zones is believed to be used in the formation of the TGO (He *et al.* 2000; Holmes & McClintock 1990; Tolpygo & Clarke 2000) during thermal cycling. The lower region of the cross-section (figure 5*a*) can be seen to have randomly distributed (bright) precipitates rich in W, Mo and Ta. Comparing with the initial microstructure in figure 1*a*, the precipitates have undergone considerable coarsening and agglomeration upon high-temperature exposure. Note that the apparent thickness of the BC has considerably increased upon thermal cycling, consistent with the observations in the past (He *et al.* 2000; Holmes & McClintock 1990). This increase is believed to be due to diffusion of Ni from the superalloy to the BC at high temperature and the subsequent decrease of the solubility of refractory elements below the BC–substrate interface (Holmes & McClintock 1990).

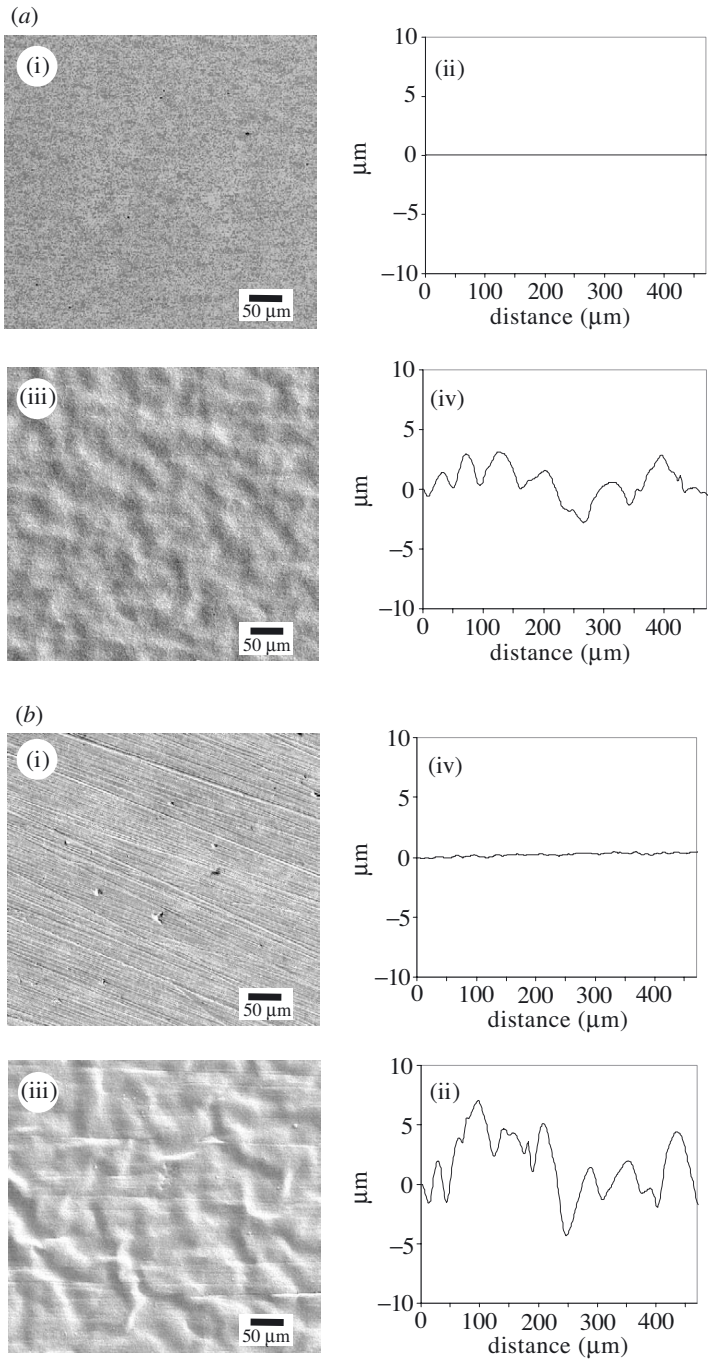

Figure 3. Representative SEM micrographs of initial and rumpled surfaces along with the corresponding profilometer scans for platinum aluminide BC. The SEM pictures and scans in (*a*)–(*d*) show BC surfaces polished successively down to 1 µm diamond paste, polished with 600 grit SiC paper, polished with 60 grit SiC paper, and in an as-deposited condition, respectively.

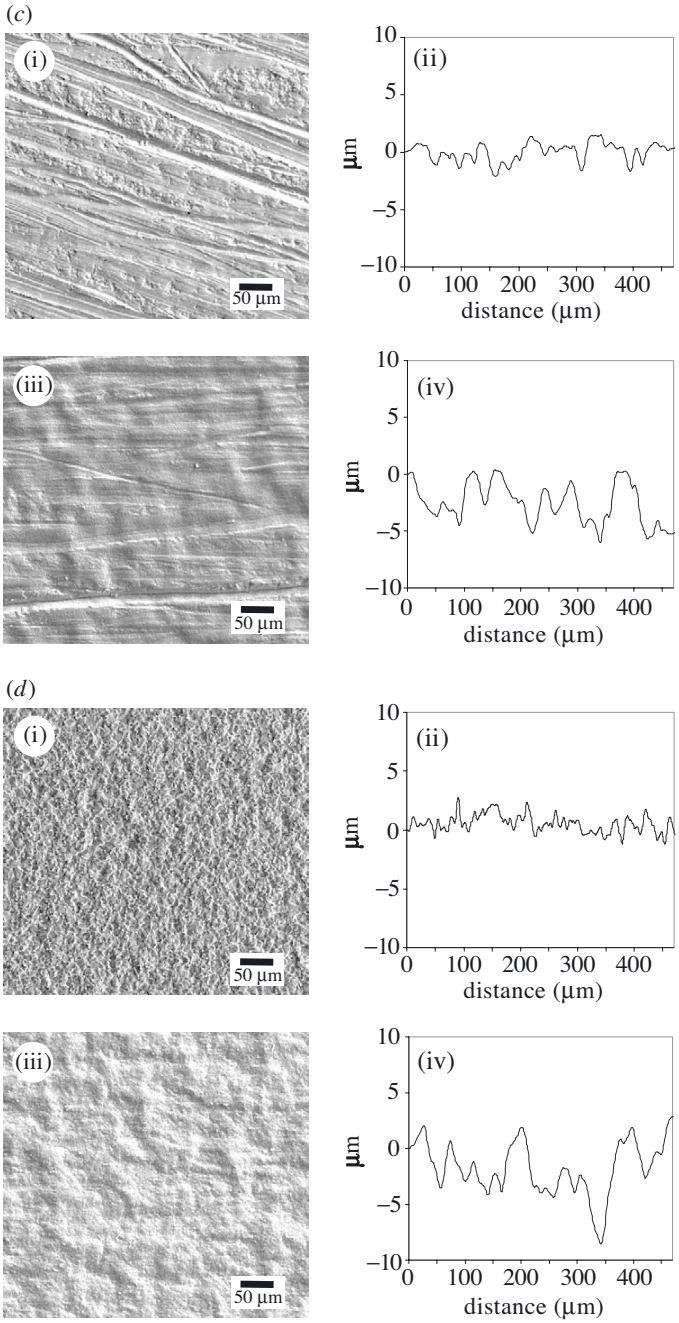

Figure 3. (*Cont.*) The profilometer scans in (*a*)(ii), (*b*)(ii), (*c*)(ii), (*d*)(ii), (*a*)(iv), (*b*)(iv), (*c*)(iv), (*d*)(iv) correspond to the BC surfaces shown in (*a*)(i), (*b*)(i), (*c*)(i), (*d*)(i), (*a*)(iii), (*b*)(iii), (*c*)(iii), (*d*)(iii), respectively. Parts (*a*)(i), (*b*)(i), (*c*)(i) and (*d*)(i) show BC surfaces before thermal cycling. After 25 thermal cycles, these surfaces become rumpled as shown in (*a*)(iii), (*b*)(iii), (*c*)(iii) and (*d*)(iii), respectively.

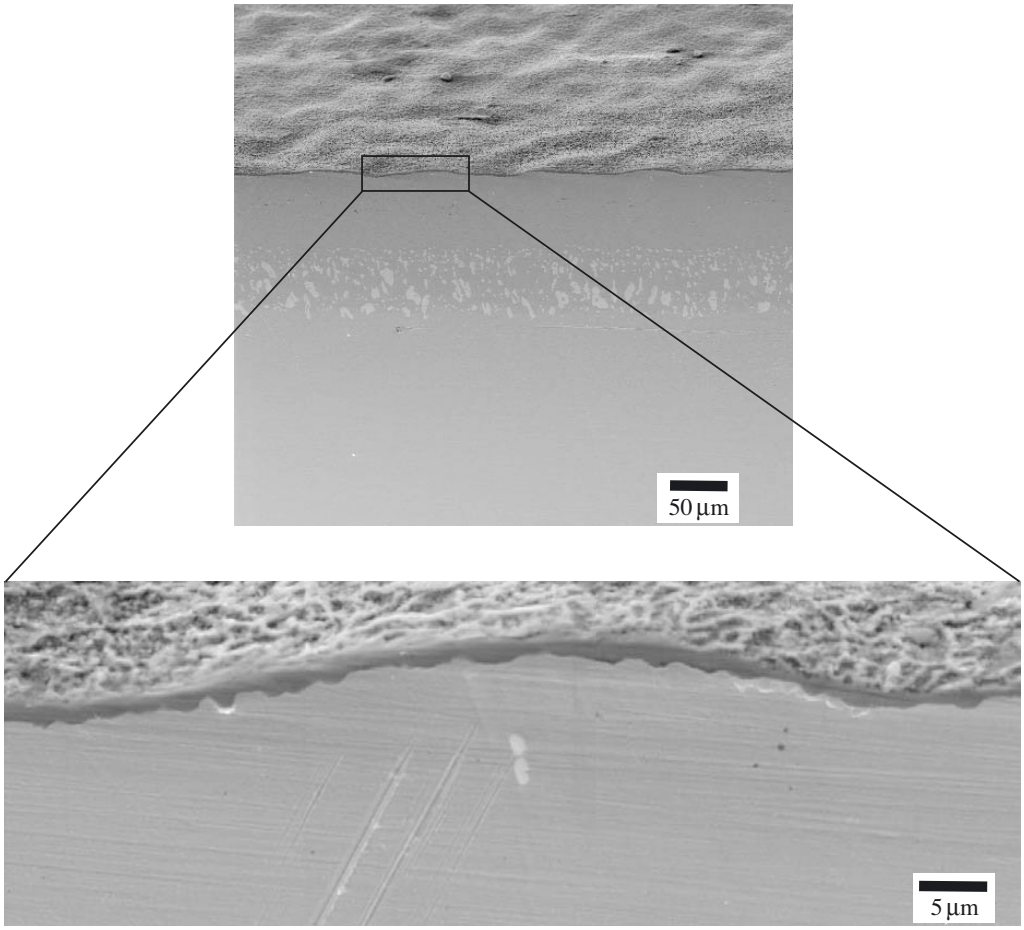

Figure 4. SEM micrograph showing the TGO morphology formed after 25 thermal cycles on the platinum aluminide BC having an initial surface polished down to 1 µm diamond paste. The micrograph is taken at a tilt of 30° to the BC cross-section.

An interesting rumpling pattern was observed near the free edge of the specimens. Figure 6*a* is an SEM micrograph of the middle region of a rumpled sample showing the random distribution of surface undulations. At the free edge, however, the rumpling ridges are distinctly aligned perpendicular to the edge, as shown in figure 6*b*. As shown schematically in figure 6*c*, the tensile stress normal to the free edge, σ_{xx}, in the BC vanishes at the edge. This stress component will gradually build up to the maximum over a distance of the order of the film thickness. In figure 6*b*, both the TGO and the BC are stress free at the edge. The extent of the 'edge zone' is, however, of the order of the BC thickness (*ca.* 100 µm).

Rumpling results for the NiCoCrAlY BC–superalloy system upon thermal cycling are shown in figure 7. The NiCoCrAlY BC surface polished down to 1 µm diamond paste is shown in figure 7*a*, *b*. It is seen in figure 7*c*, *d* that, upon 25 thermal cycles, the BC surface rumples at a wavelength about the same as that of the platinum aluminide BC. The peak-to-valley distance in the initial waviness in figure 7*a*, *b* is *ca.* 50 nm (not seen at the scale shown in the figure). The rumple amplitude of the

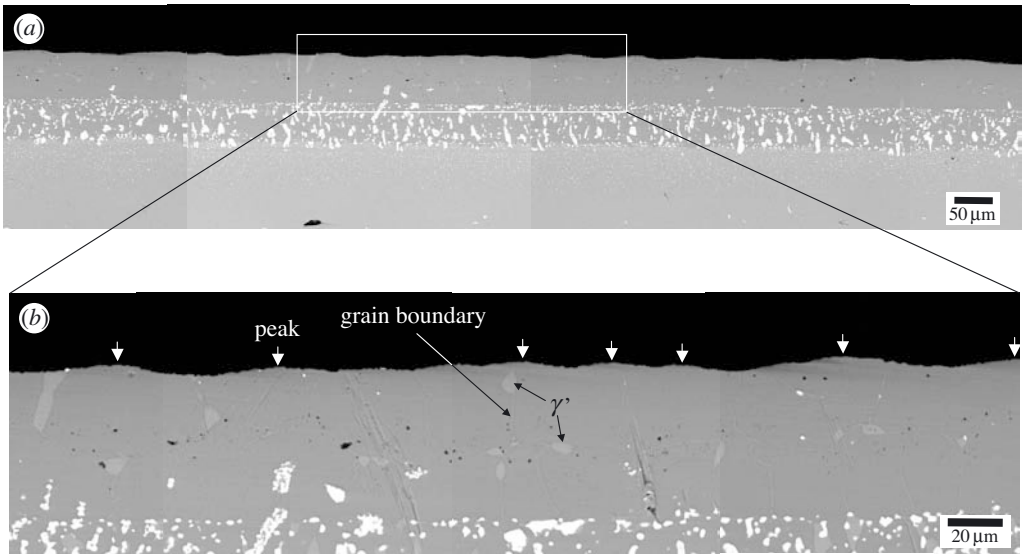

Figure 5. Representative SEM micrograph (with backscatter electrons) of BC cross-section showing the microstructure after 25 thermal cycles at different magnifications. The close-up view in (*b*) shows γ' domains along with BC grain boundaries. The white arrows indicate peaks of rumples.

NiCoCrAlY BC (figure 7*d*) is *ca.* 2 µm, smaller than that for the platinum aluminide BC (figure 3*a*(iii), (iv)) by about a factor of two. For the NiCoCrAlY BC surface polished by 600 and 60 grit SiC paper, the initial surface fluctuations were too large for the rumpling to be observed.

(ii) *Isothermal experiments in air*

Figure 8 shows a representative SEM micrograph and the corresponding profilometer scan of the surface of a platinum aluminide BC–superalloy specimen subjected to 1200 °C isothermal exposure for 25 h. As seen in figure 8*b*, the BC under isothermal exposure has rumpled with comparable rumpling amplitude and wavelength as that under thermal cycling experiments seen in figure 3*a*(iv). A representative SEM micrograph with backscatter electrons of the cross-section of the BC subjected to 1200 °C isothermal exposure for 25 h is shown in figure 9. Similar to the thermally cycled samples seen in figure 5, the BC for the isothermal experiments can be divided roughly into two regions: an upper region showing grain boundaries and a lower region consisting of bright precipitates rich in W, Mo and Ta. However, unlike the thermally cycled samples, the Al-depleted γ' regions were not seen in the upper region after isothermal treatment in figure 9. Figure 9 also shows alumina inclusions as dark regions at the boundary of the outer and the inner regions of the BC. These alumina inclusions were present before the isothermal exposure, as seen in figure 1*a*.

The rumpled surfaces seen in figures 8*a*, 3*a*(iii) and 3*b*(iii) all have a waviness with comparable wavelength and amplitude, but they appear to have a different degree of local directionality. The cause of the local directionality in rumpling patterns and

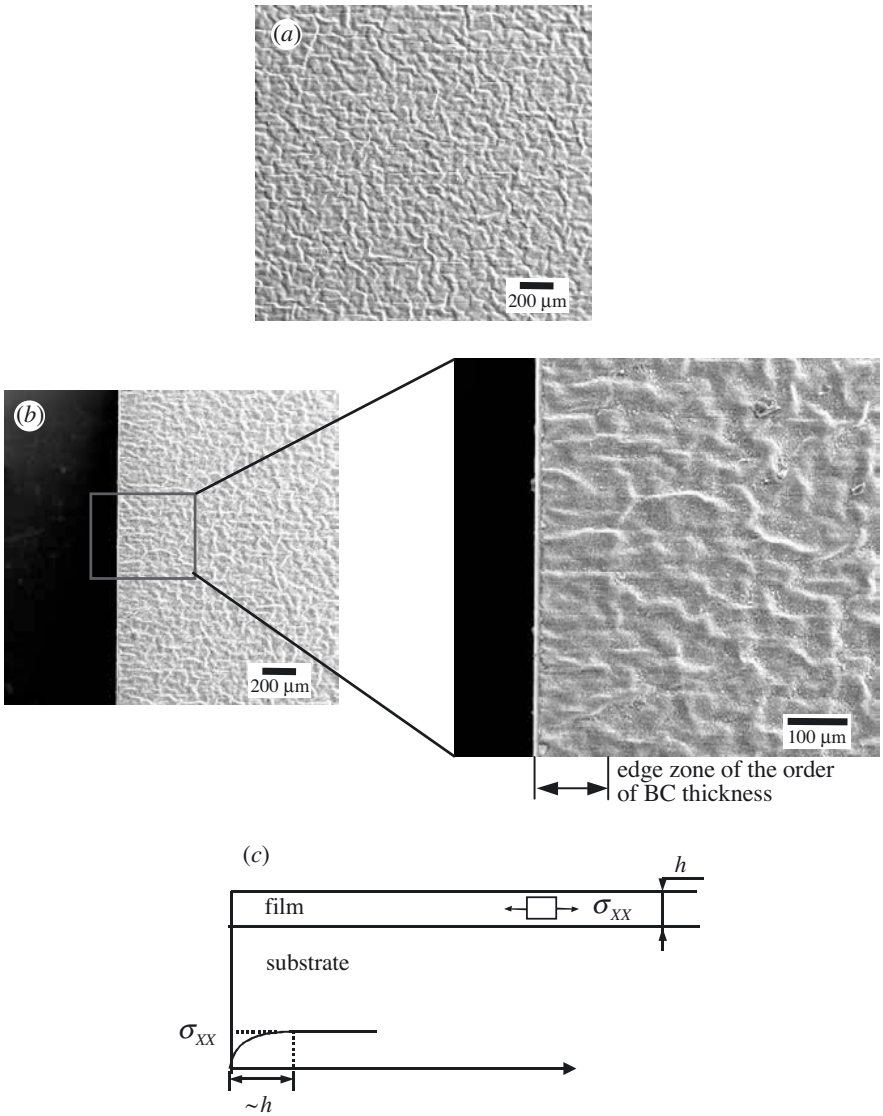

Figure 6. Rumpling (*a*) at the specimen centre and (*b*) at the specimen edge. (*c*) Expected variation of the thermal mismatch stress in a thin film. (Reprinted from Panat *et al.* (2003), with permission from Elsevier.)

its variation is not clear at present. A similar observation has been made by Tolpygo & Clarke (2000) for systems subjected to thermal cycling. Rumpling similar to that in figure 8 is observed in specimens under 1175 °C isothermal exposure for 100 h in figure 10*a*. But for isothermal experiments at 1100 and 960 °C with a hold time of 100 h, no apparent rumpling could be observed (figure 10*b*, *c*). In the case of isothermal exposure at 1175 °C for 100 h, the BC developed voids, *ca.* 10–15 µm across, near the interface between the upper and the lower regions (figure 11). These voids were irregularly placed at a distance ranging from 90 µm to 1 mm from each other.

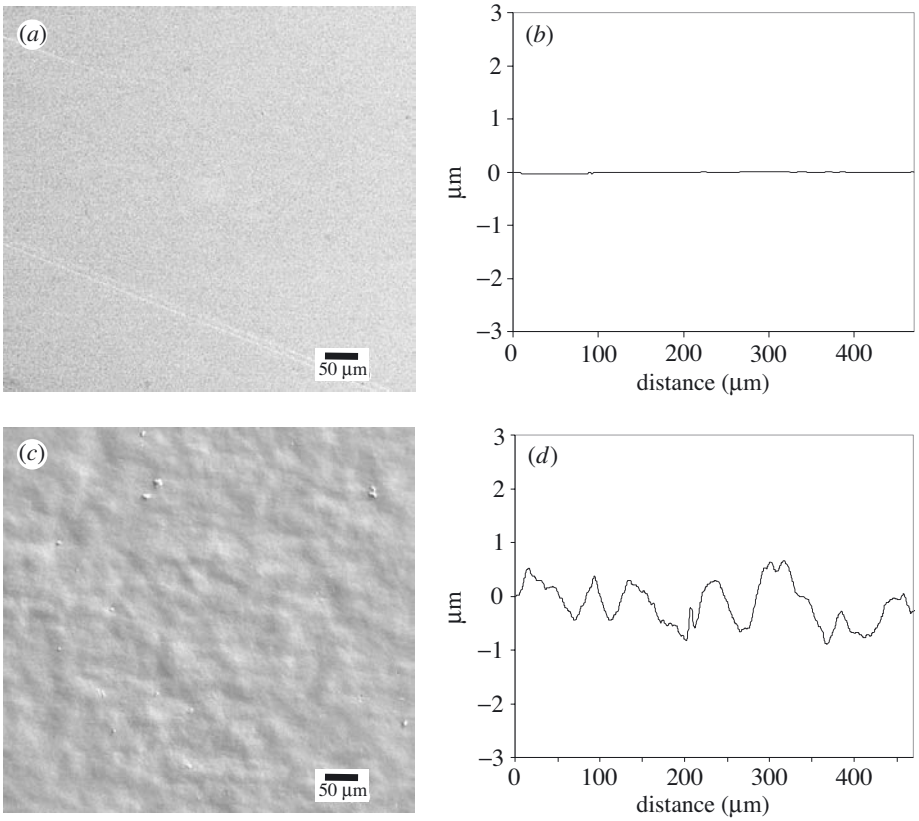

Figure 7. Representative SEM micrographs showing the top view of the NiCoCrAlY BC and corresponding profilometer scans. (*a*), (*b*) Before thermal cycling. (*c*), (*d*) After thermal cycling.

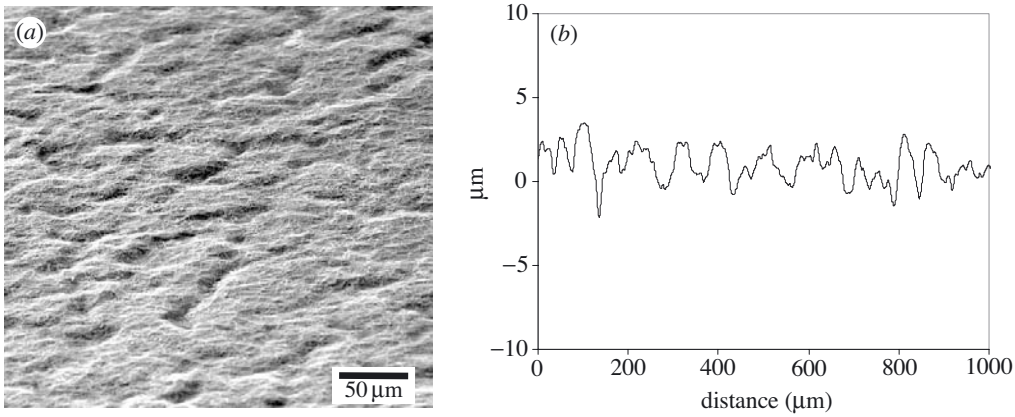

Figure 8. Top surface of platinum aluminide BC after 25 h exposure at 1200 °C. (*a*) SEM micrograph taken at 30° inclination to the cross-section; (*b*) profilometer scan.

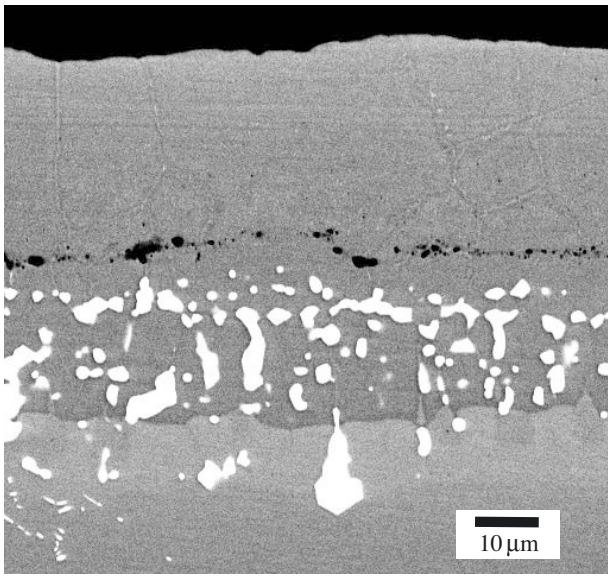

Figure 9. Representative SEM micrograph (with backscatter electrons) of platinum aluminide BC cross-section showing the microstructure after 25 h isothermal exposure at 1200 °C. Alumina inclusions can be seen as the dark regions at the boundary of the outer and the inner region of the BC. These alumina inclusions were present before the isothermal exposure (figure 1*a*).

An isolated void was observed at 1200 °C after 25 h, while at other temperatures, isothermal exposure did not result in void formation.

(iii) *Isothermal experiments in vacuum*

Figure 12 shows the result from the experiment conducted at 1200 °C for 25 h in vacuum for nickel aluminide BC. From the SEM micrograph and the corresponding profilometer scan in figure 12 it can be seen that the BC surface has rumpled upon isothermal exposure. The oxide thickness over this BC surface was estimated to be less than 10 nm from X-ray photoelectron spectroscopy (XPS) studies. This estimate was based on a comparison between the areas under the peaks representing Al in metallic form and Al in oxide (Al_2O_3) form in the X-ray intensity versus binding energy plot of the XPS of the current specimen surface (see Finnie *et al.* 2000; Strohmeier 1990). Note from figures 3 and 12 that the rumple wavelength and amplitude in the vacuum experiment are comparable to those in air.

4. Discussion

The experimental results presented in the current work elucidate several aspects of the rumpling phenomenon. It is shown that rumpling of the BC surfaces can occur under cyclic as well as isothermal temperature histories. BC surfaces with vastly different initial surface morphologies are shown to have rumpled to comparable wavelengths and amplitudes upon thermal cycling. Changes in the microstructure of the BC have been observed during rumpling. In the present section we analyse these results in the context of the existing rumpling models by He *et al.* (2000), Suo (1995), Tolpygo & Clarke (2000) and Panat *et al.* (2003).

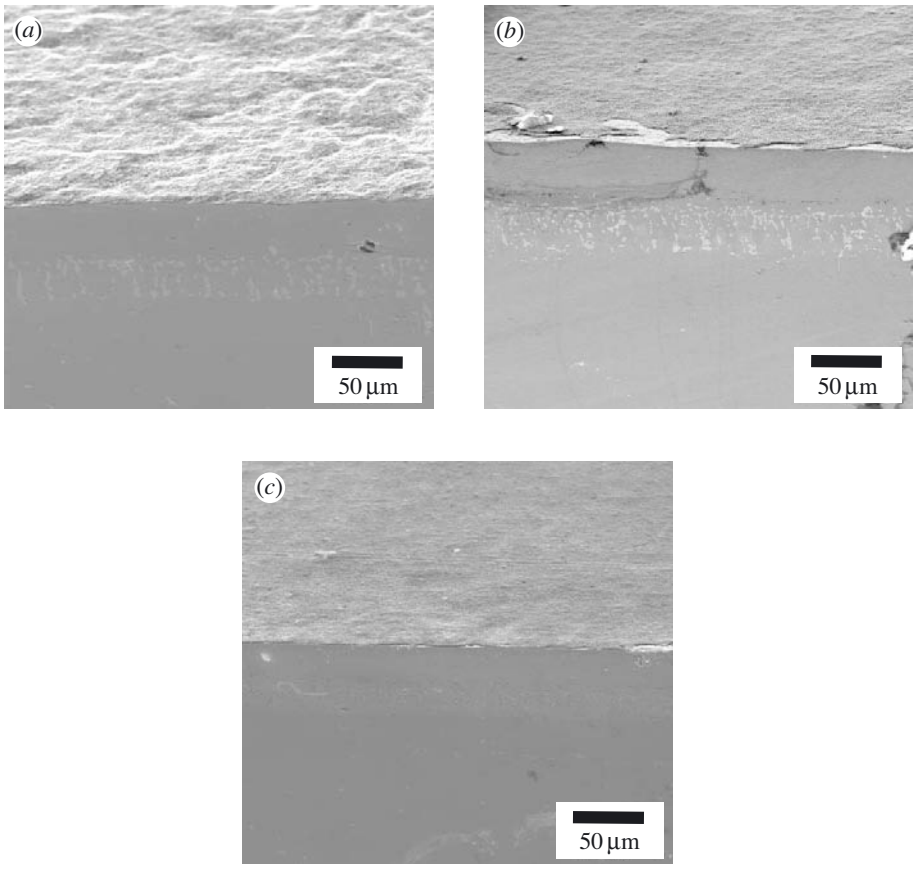

Figure 10. SEM micrographs of platinum aluminide BC after isothermal exposure for 100 h at (*a*) 1175 °C, (*d*) 1100 °C and (*e*) 960 °C. The micrographs are taken at a tilt of 30° to the BC cross-section.

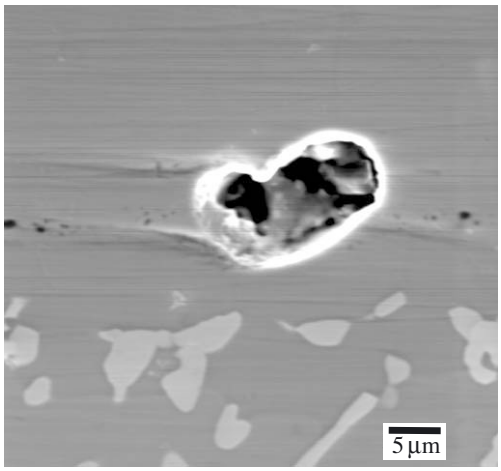

Figure 11. SEM micrograph showing an isolated void formed in platinum aluminide BC after 100 h isothermal exposure at 1175 °C.

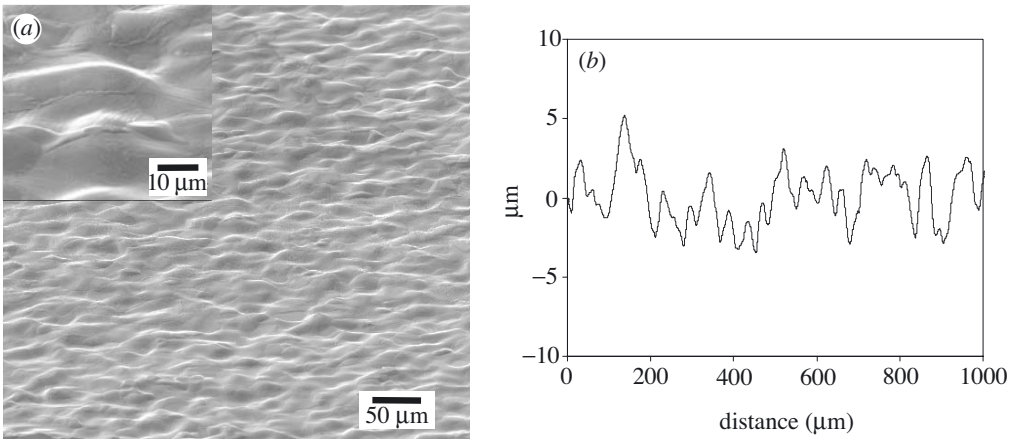

Figure 12. Nickel aluminide BC after 25 h isothermal exposure at 1200 °C in vacuum. (*a*) SEM micrograph showing BC surface rumpling; (*b*) corresponding profilometer scan. The micrograph is taken at a tilt of 30° to the BC cross-section.

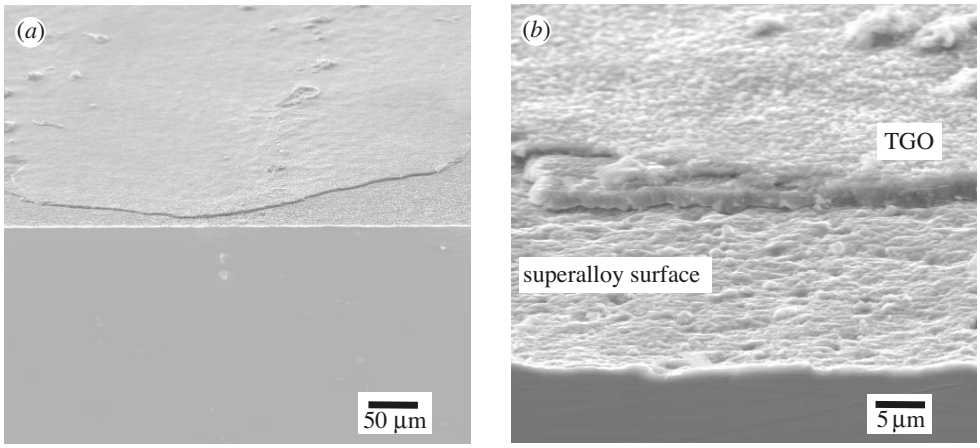

Figure 13. (*a*) SEM micrograph showing an unrumpled surface of bulk superalloy after thermal cycling. (*b*) A close-up view showing the superalloy surface, which has developed roughness during thermal cycling. Prior to thermal cycling, the superalloy surface was polished successively down to 1 µm diamond paste, similar to that in figure 3*a*(i), (ii). The micrographs are taken at a tilt of 30° to the superalloy cross-section.

(*a*) *Role of TGO in inducing BC rumpling*

Figure 13 shows SEM micrographs of a superalloy specimen without the BC subjected to identical thermal cycles as those with the BC shown in figure 4. The micrographs at different magnifications (figure 13*a*, *b*) show that the superalloy surface has not rumpled in spite of the fact that the TGO on the superalloy surface is thicker than that on the BC surface (see figure 4). Prior to thermal cycling, the superalloy surface in figure 13 was polished successively down to 1 µm diamond paste, similar to that in figure 3*a*(i), (ii). The superalloy surface exposed due to chipping of the TGO (figure 13*b*) has developed a surface roughness during thermal cycling. Note

that the TGO spallation seen in figure 13*b* occurred during cutting of the specimen after the thermal cycling experiment.

Under thermal cycling of the bulk superalloy, the TGO stresses alone are expected to be dominant; while for the BC on the superalloy, the stresses in both the BC and the TGO might be important. Figure 13 demonstrates that the presence of BC is critical for the rumpling to occur. Moreover, we observed from figure 3 that initial flaws of certain amplitude were not necessary to cause the BC surface to rumple, as required by the TGO-driven ratcheting model of He *et al.* (2000). These experiments suggest that the role of the TGO is limited in inducing the long-range rumpling seen in the present work and previous studies (e.g. Deb *et al.* 1987; Holmes & McClintock 1990; Pennefather & Boone 1995; Tolpygo & Clarke 2000; Zhang *et al.* 1999).

In fact, TGO of a few micrometres thick is not likely to result in rumpling with wavelengths of the order of 100 μm. Similar inference has been drawn by Suo (1995) and by Tolpygo & Clarke (2000). Suo (1995) suggests that his TGO stress-driven diffusion model coupled with TGO growth kinetics would cause a metal substrate to rumple with wavelengths of a few times the TGO thickness (Tolpygo & Grabke 1994). Note that the small-scale waviness observed in the present work (figure 4) does indeed have a wavelength that is a few times the TGO thickness. Tolpygo & Clarke (2000) have reported that significant difference in the levels of TGO stresses at room temperature has no quantitative effect in the resulting BC rumpling amplitudes and wavelengths, further indicating a limited role for TGO in determining the rumpling behaviour.

A further confirmation of this inference can be seen in the rumpling observed for nickel aluminide BC in figure 12 under vacuum environment. The TGO with a thickness less than 10 nm over this BC surface cannot possibly be the cause of BC rumpling to the wavelengths seen in figure 12. Figures 3 and 12 show that the rumpling wavelengths and amplitudes in the vacuum experiment are comparable with those in air, confirming again that TGO is not needed to induce the long-range rumpling. For thicker TGOs developed in these systems, the TGO stress may play an important role in the system behaviour. In the presence of the TBC, the BC is shown to develop conical 'depressions' or 'instability sites' upon thermal cycling (Mumm *et al.* 2001; Ruud *et al.* 2001). These sites that affect TBC life (Ruud *et al.* 2001) have a characteristic dimension of a few times the TGO thickness. The TGO stresses may play an important role in their development (Karlsson & Evans 2001). The role of the TGO growth stresses in the development of the small-scale waviness observed in the current experiments (figure 4) needs further work.

(*b*) *The role of BC microstructural changes in inducing BC rumpling*

Tolpygo & Clarke (2000) suggested that the rumpling behaviour is related to the microstructural changes in the BC. Particularly, the roles of the γ' phase formed in the BC under cyclic oxidation and the voids formed in the BC under isothermal oxidation have been emphasized. It was suggested that rumpling and void formation may be different manifestations of the same form of a common volume-depletion process. To check the validity of this argument, we analysed figure 5 for a possible correlation between the microstructural evolution and BC rumpling behaviour. Figure 14 shows the number of occurrences of the Al-depleted γ' phase in the BC cross-section in figure 5*a*, as a function of their relative locations with respect to the

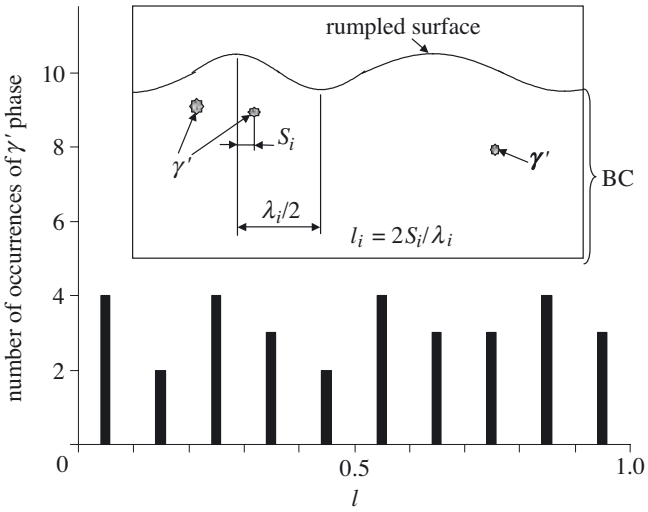

Figure 14. Occurrence of the γ' phase relative to the rumples in figure 5. The schematic in the insert shows the method of calculating the γ' phase occurrence with respect to the rumpled surface.

rumple peak and the adjacent rumple valley. If the distance between a peak and the nearest γ' region is S_i, the normalized distance l_i is calculated by

$$l_i = 2\left(\frac{S_i}{\lambda_i}\right), \tag{4.1}$$

where λ_i is the wavelength of the surface undulation at the occurrence of the γ' phase, as shown in figure 14. It is clear that the γ' phase coincides with the peak when the normalized distance $l \approx 0$, or with the valley when $l \approx 1$. Figure 14 shows that the γ' phase is not preferentially oriented either towards the valleys or towards the peaks of the rumples. A further look at figure 5 reveals that the occurrence of bright regions representing the precipitates rich in W, Mo and Ta have a poor correlation with the occurrence of the rumples. Note also that prior to thermal cycling, the microstructural periodicity associated with the precipitates in the IDZ of the platinum aluminide BC is *ca.* 2–3 μm (figure 1*a*), while that associated with the bright and dark regions in NiCoCrAlY BC is *ca.* 3–4 μm (figure 1*d*), much smaller than the rumple wavelengths seen in experiments (figures 3 and 7). These observations indicate that the microstructural changes occurring in the BC are not strongly correlated with the rumpling phenomenon. A study of TBC systems by Mumm *et al.* (2001) with a similar BC as in the present work has also shown a poor correlation between the occurrence of γ' domains and BC instability sites (i.e. valleys in the presence of the ceramic topcoat) in their experiments.

Furthermore, the isothermal experimental results at 1175 °C, shown in figures 10*a* and 11, indicate that the distance between these voids (90 μm to 1 mm) did not correspond well with the rumple wavelength. It should be recognized that void formation under isothermal conditions is an important phenomenon that may influence TBC failure (Tolpygo & Clarke 2001). However, the relationship between BC rumpling and void formation is not well established.

(*c*) *BC stress-driven deformation mechanisms*

The above discussion in §§ 4 *a* and 4 *b* and the result in § 3 *a* (ii) on the extent of the 'edge zone' demonstrate that the stresses in the BC provide the driving force for rumpling formation. In this section, we discuss the deformation and mass-transport mechanisms that give rise to the rumpled surface in the BC. These mechanisms could include volume diffusion, surface diffusion (see Panat *et al.* 2003), dislocation creep, or a combination of these processes. In particular, we focus our discussion on one such possible mechanism, the BC stress-driven surface diffusion, which was proposed by the present authors (Panat *et al.* 2003).

The model by Panat *et al.* (2003) predicts that the rumpling behaviour should be relatively insensitive to the initial surface fluctuations as long as the amplitudes of the initial fluctuations are significantly smaller than the thickness of the BC. Our experimental observations in figure 3 demonstrate that vastly different initial surfaces with roughness from tens of nanometres to a few micrometres will all evolve into similar rumpled surfaces upon thermal cycling. The model by Panat *et al.* (2003), using estimates of material parameters from the literature (Freund 1995; Karlsson & Evans 2001), predicts that the characteristic wavelength of the rumpled surfaces is *ca.* 100–250 μm, which is also consistent with the measured rumpling wavelengths in the present work as well as in other researchers' observations (Deb *et al.* 1987; Holmes & McClintock 1990; Pennefather & Boone 1995; Tolpygo & Clarke 2000; Zhang *et al.* 1999).

The source of the stresses in the BC is believed to be the thermal expansion mismatch between the BC and the substrate materials. As a result, the model by Panat *et al.* (2003) does not discriminate between cyclic thermal and isothermal histories. As long as the temperature is sufficiently different from the BC processing temperature such that enough mismatch stress exists in the BC, rumpling will occur. Indeed our experiments show that, under isothermal conditions at 1200 °C and 1175 °C in air and at 1200 °C in vacuum, BC surface rumpling occurs with comparable amplitudes and wavelengths as those subjected to cyclic thermal history. However, our isothermal experiments at 1100 and 960 °C for 100 h did not result in any rumpling of the BC surface, neither did the isothermal experiments of Tolpygo & Clarke (2000) or Deb *et al.* (1987) at 1150 and 1100 °C, respectively.

Using the model of Panat *et al.* (2003), we estimated the time required, at different isothermal heating temperatures, to generate the waviness of the same magnitude as that subjected to 1200 °C exposure. The result is shown in figure 15. The biggest uncertainty in generating this figure is the BC processing temperature, i.e. the 'stress-free temperature'. Based on the BC processing parameters of the current specimens, we considered several processing temperatures in figure 15. The plot indicates that, at a given isothermal heating temperature, rumpling of the same amplitude as that obtained at 1200 °C for 25 h can be achieved after the heating time dictated by the curves. Different curves indicate that different heating times are needed if the processing temperature is different. The solid and open symbols are our and other researchers' experimental results. The solid symbols represent the experiments in which rumpling has occurred, whereas open symbols indicate no rumpling. Figure 15 shows that if the processing temperature is *ca.* 1050 °C, rumpling will occur after 25 h exposure at 1200 °C or after 100 h at 1175 °C. However, for the BC surface to generate a comparable rumpling at 1150 °C, *ca.* 780 h of heating time is needed,

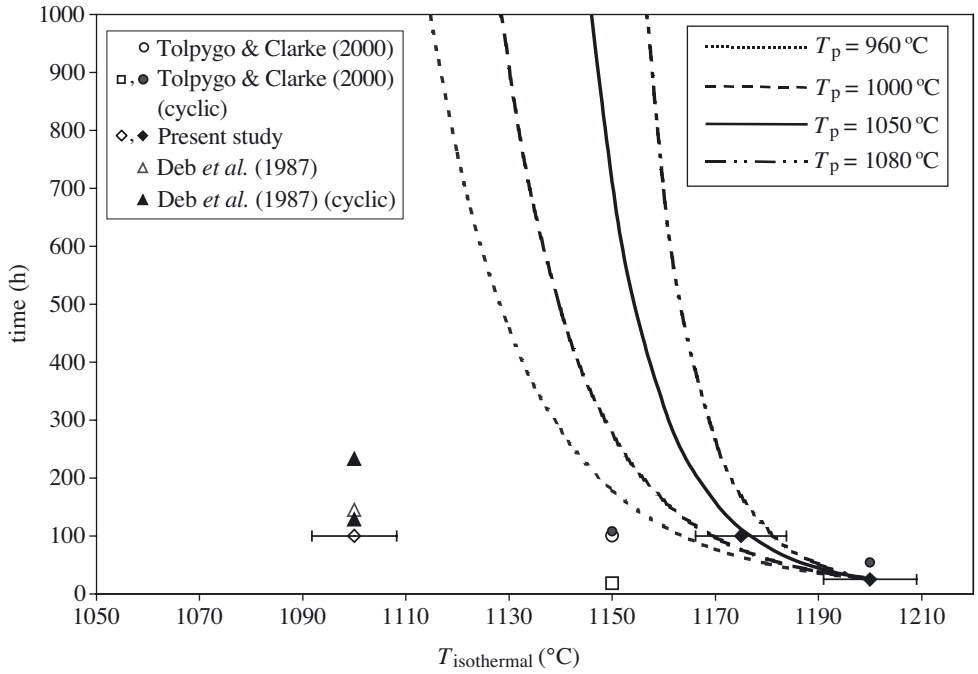

Figure 15. Time required to reach the comparable rumpling amplitude as that at 1200 °C after 25 h for different processing temperatures based on the BC stress-driven surface-diffusion model by Panat *et al.* (2003). The open symbols indicate that BC rumpling did not occur, while the filled symbols indicate that BC rumpling occurred.

substantially longer than the exposure time used by Tolpygo & Clarke (2000). The exposure times of our isothermal experiments at 1100 and 960 °C, as well as other researchers' experiments at 1100 °C (Deb *et al.* 1987), are all far shorter than what is needed to produce reasonable rumpling of the BC surface.

To compare the isothermal results with those with cyclic temperature history, we plot in figure 15 the data from the literature (Deb *et al.* 1987; Tolpygo & Clarke 2000) for platinum aluminide BCs subjected to thermal cycling with fast heating and cooling rates. The equivalent heating times of their experiments were calculated by the sum of the holding times at high temperature and a weighted average of the heating and cooling times. This comparison shows that the model of Panat *et al.* (2003) cannot fully resolve the difference between isothermal heating and thermal cycling, especially for the data from Deb *et al.* (1987). We speculate that other mechanisms such as plastic deformation or creep may be contributing to the rumpling process, or the TGO could have some effect on rumpling. These are factors not taken into account by Panat *et al.* (2003). We know, however, from our experiments in vacuum that rumpling can occur in the absence of any significant oxidation. Further research, both modelling and experimental, is needed to obtain a complete picture of the rumpling behaviour in thermal barrier systems. Note that, in generating figure 15, we assumed that the specific diffusivity D_0 and the activation energy q for surface diffusion in the BC remain constant at all temperature levels, which may not be true, especially at lower temperatures.

Recently, Suo *et al.* (2003) have found that after 300 h exposure at 1150 °C, the BC develops extensive voids near the surface. The void formation was attributed to the diffusion of BC constituents perpendicular to the BC top surface (Suo *et al.* 2003). Clearly, void formation appears to dominate the BC behaviour at 1150 °C after a long time. It is conceivable that different mechanisms may be dominant at different temperatures during high-temperature exposure. We are currently conducting experiments in vacuum and in air to investigate the dominant processes in BC for several temperature ranges. Extensive experimental observations are needed to obtain a 'mechanism map' in these systems that can show a complete picture of the behaviour of BC systems at high temperatures. Such a map can then be used to enhance their performance in TBCs.

5. Conclusions

In the present work, isothermal and cyclic thermal experiments are carried out on BC–superalloy systems. The results indicate the following.

(i) The driving force for rumpling formation is likely to be the thermal mismatch stress in the BC.

(ii) Rumpling can occur under both thermal cycling and isothermal heating conditions.

(iii) Rumpling wavelength is relatively insensitive to initial BC surface fluctuations. Significant initial flaws are not needed for rumpling to occur.

(iv) TGO plays a limited role in BC surface rumpling behaviour. Rumpling occurs even in the absence of oxidation when experiments are conducted in vacuum.

(v) Several microstructural changes occur in the BC during rumpling. These changes are found to have a poor correlation with the periodicity associated with rumpling.

(vi) Rumpling behaviour under isothermal conditions depends upon the hold temperature and time.

(vii) Several deformation mechanisms are plausible for rumpling formation, including surface/bulk/grain boundary diffusion, dislocation creep, and plastic deformation. The rumpling features observed in the present study can be explained by a BC stress-driven surface-diffusion model (Panat *et al.* 2003).

This work is supported by a Critical Research Initiative programme at the University of Illinois at Urbana-Champaign (UIUC). Thanks go to Dr Ram Darolia of General Electric for providing the superalloys. Thanks also go to the Paul Lawton, Stacy Fang and Anthony Collucci of Chromalloy, NY, for coating the superalloys with the bond coat. The SEM, XRD and profilometry work was carried out in the Center for Microanalysis of Materials, Frederick Seitz Materials Research Laboratory, UIUC, which is partially supported by the US Department of Energy under grant DEFG02-91-ER45439. The authors acknowledge helpful discussions with Professor T.-C. Chiang, Dr Rick Haasch, Dr Sulin Zhang and Ming Liu at UIUC. Discussion with Professor J. W. Hutchinson is also acknowledged. Finally, thanks go to the anonymous reviewer for his/her helpful comments.

References

Ambrico, J. M., Begley, M. & Jordan, E. H. 2001 Stress and shape evolution in oxide films on elastic-plastic substrates due to thermal cycling and film growth. *Acta Mater.* **49**, 1577–1588.

Bouhanek, K., Adesanya, O. A., Stott, F. H., Skeldon, P., Lees, D. G. & Wood, G. C. 2000 Isothermal and thermal cyclic oxidation behavior of thermal barrier coatings: Pt aluminide bond coat. *Mater. High Temp.* **2**, 185–196.

Deb, P., Boone, D. H. & Manley, T. F. I. 1987 Surface instability of platinum modified aluminized coatings during 1100 °C cyclic testing. *J. Vac. Sci. Technol.* **5**, 3366–3372.

Evans, A. G., Mumm, D. R., Hutchinson, J. W., Meier, G. H. & Pettit, F. S. 2001 Mechanisms controlling the durability of thermal barrier coatings. *Prog. Mater. Sci.* **46**, 505–553.

Finnie, K. R., Haasch, R. & Nuzzo, R. G. 2000 Formation and patterning of self-assembled monolayers driven from long-chain organosilicon amphiphiles and their use as templates in materials microfabrication. *Langmuir* **16**, 6968–6976.

Freund, L. B. 1995 Evolution of waviness on the surface of a strained elastic solid due to stress-driven diffusion. *Int. J. Solids Struct.* **32**, 911–923.

Goward, G. W. 1998 Progress in coatings for gas turbine airfoils. *Surf. Coat. Technol.* **108–109**, 73–79.

He, M. Y., Evans, A. G. & Hutchinson, J. W. 2000 The ratcheting of compressed thermally grown thin films on ductile substrates. *Acta Mater.* **48**, 2593–2601.

Holmes, J. W. & McClintock, F. A. 1990 The chemical and mechanical processes of thermal fatigue degradation of an aluminide coating. *Metall. Trans.* A **21**, 1209–1222.

Ibegazene-Ouali, F., Mervel, R., Rio, C. & Renollet, Y. 2000 Microstructural evolution and degradation modes in cyclic and isothermal oxidation of an EB–PVD thermal barrier coating. *Mater. High Temp.* **17**, 205–218.

Karlsson, A. M. & Evans, A. G. 2001 A numerical model for the cyclic instability of thermally grown oxides in thermal barrier coatings. *Acta Mater.* **49**, 1793–1804.

Karlsson, A. M., Hutchinson, J. W. & Evans, A. G. 2002 Fundamental model of cyclic instabilities in thermal barrier systems. *J. Mech. Phys. Solids* **50**, 1565–1589.

Levy, A. V. & MacAdam, S. 1988 Durability of ceramic coatings in 14 000 hours service in a marine diesel engine. ASME Paper, no. 88-ICE-19. New York: ASME Press.

Meier, S. M. & Gupta, D. K. 1994 The evolution of thermal barrier coatings in gas turbine engine applications. *J. Engng Gas Turbines Power* **116**, 250–257.

Miller, R. A. 1987 Current status of thermal barrier coatings—an overview. *Surf. Coat. Technol.* **30**, 1–11.

Mumm, D. R., Evans, A. G. & Spitsberg, I. T. 2001 Characterization of a cyclic displacement instability for a thermally grown oxide in a thermal barrier system. *Acta Mater.* **49**, 2329–2340.

Padture, N. P., Gell, M. & Jordan, E. H. 2002 Thermal barrier coatings for gas-turbine engine applications. *Science* **296**, 280–284.

Panat, R. P., Zhang, S. & Hsia, K. J. 2003 Bond coat surface rumpling in thermal barrier coatings. *Acta Mater.* **51**, 239–249.

Pennefather, R. C. & Boone, D. H. 1995 Mechanical degradation of coating system in high-temperature cyclic oxidation. *Surf. Coat. Technol.* **76–77**, 47–52.

Rejda, E. F., Socie, D. F. & Itoh, T. 1999 Deformation behavior of plasma-sprayed thick thermal barrier coatings. *Surf. Coat. Technol.* **113**, 218–226.

Ruud, J. A., Bartz, A., Borom, M. P. & Johnson, C. A. 2001 Strength degradation and failure mechanisms of electron-beam-physical-vapor-deposited thermal barrier coatings. *J. Am. Ceram. Soc.* **84**, 1545–1552.

Schulz, U., Menzebach, M., Leyens, C. & Yang, Y. Q. 2001 Influence of substrate material on oxidation behavior and cyclic lifetime of EB–PVD TBC systems. *Surf. Coat. Technol.* **146–147**, 117–123.

Schulz, U., Leyens, C., Fritscher, K., Peters, M., Saruhan-Brings, B., Lavigne, O., Dorvaux, J., Poulain, M., Mevrel, R. & Calez, M. 2003 Some recent trends in research and technology of advanced thermal barrier coatings. *Aerospace Sci. Technol.* **7**, 73–80.

Sheffler, K. D. & Gupta, D. K. 1988 Current status and future trends in turbine applications of thermal barrier coatings. *J. Engng Gas Turbines Power* **110**, 605–609.

Sohn, Y. H., Kim, J. H., Jordan, E. H. & Gell, M. 2001 Thermal cycling of EB–PVD/MCRALY thermal barrier coatings. I. Microstructural development and spallation mechanisms. *Surf. Coat. Technol.* **146–147**, 70–78.

Stiger, M. J., Yanar, N. M., Topping, M. G., Pettit, F. S. & Meier, G. H. 1999 Thermal barrier coatings for the 21st century. *Z. Metallk.* **90**, 1069–1078.

Strangman, T. E. 1985 Thermal barrier coatings for turbine airfoils. *Thin Solid Films* **127**, 93–106.

Strohmeier, B. 1990 An ESCA method for determining the oxide thickness on aluminum alloys. *Surf. Interf. Analysis* **15**, 51–56.

Suo, Z. 1995 Wrinkling of the oxide scale on an aluminium-containing alloy at high temperatures. *J. Mech. Phys. Solids* **43**, 829–846.

Suo, Z., Kubair, D., Evans, A. G., Clarke, D. R. & Tolpygo, V. 2003 Stresses induced in alloys by selective oxidation. *Acta Mater.* **51**, 959–974.

Tolpygo, V. K. & Clarke, D. R. 2000 Surface rumpling of a (Ni,Pt)Al bond coat induced by cyclic oxidation. *Acta Mater.* **48**, 3283–3293.

Tolpygo, V. K. & Clarke, D. R. 2001 Damage induced by thermal cycling of thermal barrier coatings. In *Elevated temperature coatings: science and technology* (ed. N. B. Dahotre, J. M. Hampikian & J. E. Morral), vol. IV, p. 94. Warrendale, PA: The Minerals, Metals and Materials Society.

Tolpygo, V. K. & Grabke, H. J. 1994 Microstructural characterization and adherence of the α-Al_2O_3 oxide scale on the Fe–Cr–Al and Fe–Cr–Al–Y alloys. *Oxid. Metals* **41**, 343–2601.

Tolpygo, V. K., Clarke, D. R. & Murphy, K. S. 2001 Oxidation induced failure of EB–PVD thermal barrier coatings. *Surf. Coat. Technol.* **146–147**, 124–134.

Vaidyanathan, K., Gell, M. & Jordan, E. 2000 Mechanisms of spallation of electron beam physical vapor deposited thermal barrier coatings with and without platinum aluminide bond coat ridges. *Surf. Coat. Technol.* **133–134**, 28–34.

Walston, W. S., O'Hara, K. S., Ross, E. W., Pollock, T. M. & Murphy, W. H. 1996 Ren'e N6: third generation single crystal superalloy. In *Proc. Superalloys Symposium* (ed. R. D. Kissinger, D. J. Deye, D. L. Anton, A. D. Cetel, M. V. Nathal, T. M. Pollock & D. A. Woodford), pp. 27–33. Warrendale, PA: The Minerals, Metals and Materials Society.

Wright, P. K. 1998 Influence of cyclic strain on life of a PVD TBC. *Mater. Sci. Engng* A **245**, 191–200.

Wright, P. K. & Evans, A. G. 1999 Mechanisms governing the performance of thermal barrier coatings. *Curr. Opin. Solid State Mater. Sci.* **4**, 255–265.

Wu, B. C., Chang, E., Chang, S. F. & Chao, C. H. 1989 Thermal cyclic response of yttria-stabilized zirconia/CoNiCrAlY thermal barrier coatings. *Thin Solid Films* **172**, 185–196.

Zhang, Y. H., Withers, P. J., Fox, M. D. & Knowles, D. M. 1999 Damage mechanisms of coated systems under thermomechanical fatigue. *Mater. Sci. Technol.* **15**, 1031–1036.